RESEARCH LETTER

Key Points:
- We observe cyclic pore-scale behavior of supercritical CO_2 (scCO_2) via synchrotron X-ray microtomography
- Residual scCO_2 saturation increases over multiple drainage-imbibition (D-I) cycles reaching a value of 50% after three cycles
- The ultimate driver for this behavior may be a combination of cycling and associated surface chemistry reactions

Supporting Information:
- Supporting Information S1

Correspondence to:
A. L. Herring,
Anna.herring@anu.edu.au

Enhancing residual trapping of supercritical CO₂ via cyclic injections

Anna L. Herring[1,2], Linnéa Andersson[1], and Dorthe Wildenschild[1]

[1]School of Chemical, Biological and Environmental Engineering, Oregon State University, Corvallis, Oregon, USA, [2]Department of Applied Mathematics, Research School of Physics and Engineering, Australian National University, Canberra, Australian Capital Territory, Australia

Abstract We utilize synchrotron X-ray tomographic imaging to investigate the pore-scale characteristics and residual trapping of supercritical CO_2 (scCO_2) over the course of multiple drainage-imbibition (D-I) cycles in Bentheimer sandstone cores. Capillary pressure measurements are paired with X-ray image-derived saturation and connectivity metrics which describe the extent of drainage and subsequent residual (end of imbibition) scCO_2 trapping. For the first D-I cycle, residual scCO_2 trapping is suppressed due to high imbibition capillary number (Ca $\approx 10^{-6}$); however, residual scCO_2 trapping dramatically increases for subsequent D-I cycles carried out at the same Ca value. This behavior is not predicted by conventional multiphase trapping theory. The magnitude of scCO_2 trapping increase is hysteretic and depends on the relative extent of the sequential drainage processes. The hysteretic pore-scale behavior of the scCO_2-brine-sandstone system observed in this study suggests that cyclic multiphase flow could potentially be used to increase scCO_2 trapping for sequestration applications.

1. Introduction

Multiphase flow of supercritical carbon dioxide (CO_2) and brine within porous media has recently been a topic of intensive research for application to carbon capture and storage (CCS), a climate change mitigation strategy. During CCS operations, CO_2 is first captured from the waste stream of a large point source of carbon emissions (e.g., a coal-fired power plant), then pressurized and injected into the subsurface. As the pressurized CO_2 is pumped underground, it warms to in situ temperature of the storage reservoir; under the pressure and temperature conditions of most reservoirs targeted for CO_2 sequestration, the injected CO_2 will exist in a supercritical state (denoted scCO_2 in the present study) [*Intergovernmental Panel on Climate Change*, 2005; *Benson and Cole*, 2008]. Sandstones and other sedimentary formations provide favorable storage conditions [*Bachu*, 2003; *Gunter et al.*, 2004]; and although wettability measurements of scCO_2-brine-geologic media systems are thus far inconclusive [*Wan et al.*, 2014], for sandstone formations, aqueous brine has been observed to be the dominant wetting phase while scCO_2 is the nonwetting phase [*Pentland et al.*, 2011; *Krevor et al.*, 2012; *Pini and Benson*, 2013; *Herring et al.*, 2014; *Kaveh et al.*, 2014]; these observations are supported by measurements of water-wet (or weakly water-wet) contact angles on surfaces representative of sandstones [*Chaudhary et al.*, 2015]. The nomenclature used in the following reflects this assumption of water-wet porous media.

Of particular importance to the storage safety and success of a sequestration operation is the amount of scCO_2 which is immobilized by "residual" or "capillary" trapping, that is, the amount of scCO_2 trapped as isolated ganglion in rock pores after the completion of scCO_2 injection (a drainage process) and subsequent brine reinvasion (imbibition). The residual trapping mechanism hinders large-scale mobilization of scCO_2 in the subsurface, reducing the possibility of upward CO_2 migration and accidental release to groundwater or the atmosphere and also breaks up the relatively large continuous scCO_2 plume into many small ganglia with larger surface area to volume ratios, thus enhancing long-term dissolution and precipitation reactions which further improves storage security.

Numerous experimental studies have been conducted to investigate immiscible scCO_2 flow and residual trapping behavior at the pore-to-core (i.e., μm to cm) scale within porous media such as two dimensional (2-D) micromodels [*Wang et al.*, 2012; *Kazemifar et al.*, 2015], bead columns [*Chaudhary et al.*, 2013], sand packs [*Plug and Bruining*, 2007], sandstones [*Bachu and Bennion*, 2008; *Al Mansoori et al.*, 2009; *Perrin and Benson*, 2010; *Iglauer et al.*, 2011; *Akbarabadi and Piri*, 2013; *Ruprecht et al.*, 2014; *Herring et al.*, 2014;

Reynolds et al., 2014; *Manceau et al.*, 2015; *Niu et al.*, 2015; *Reynolds and Krevor*, 2015], shales [*Bachu and Bennion*, 2008], and carbonates [*Bachu and Bennion*, 2008; *Andrew et al.*, 2013, 2014; *El-Maghraby and Blunt*, 2013]. On larger scales, ambient condition studies using analogue fluids and gaseous CO_2 have been performed at the meter scale [*Plampin et al.*, 2014; *Trevisan et al.*, 2014], and modeling simulations have been utilized to predict basin-scale transport and fate of injected $scCO_2$ plumes [*Spiteri et al.*, 2005; *Juanes et al.*, 2006, 2010; *Kumar et al.*, 2005].

While extensive characterization has been carried out on the primary flow processes, i.e., primary drainage and main imbibition, the potential for repeated drainage-imbibition (D-I) processes (injection-waterflood) during geologic sequestration and the hysteretic nature of multiphase flow processes necessitate further investigation of the trapping potential of multiple D-I cycles on $scCO_2$ flow and trapping. Results from reservoir condition core-scale experiments consisting of three D-I cycles indicate that although measured pressure profiles and relative permeability are cycle dependent parameters, cycle number has no discernible impact on residual $scCO_2$ saturations [*Saeedi et al.*, 2011]; a similar result was found by *Li et al.* [2015], who measured initial-residual saturation levels over two D-I cycles in Berea sandstone and found that the results conformed to the expected monotonic trapping curve. This conclusion has been echoed by ambient condition experiments that indicate that residual trapping is limited by the shape of the main imbibition curve [*Raeesi et al.*, 2014]. In contrast, results from recent pore-scale studies have suggested that intermittent injection patterns, or cyclic injections similar to water-alternating-gas schemes, could be utilized to break up the $scCO_2$ plume and enhance residual trapping of $scCO_2$ [*Herring et al.*, 2013, 2015]; cyclic injection schemes have also previously been suggested by researchers performing basin-scale simulations [*Spiteri et al.*, 2005]. Additional studies of $scCO_2$ flow processes have produced observations of time-dependent wettability alteration [*Kim et al.*, 2012; *Wang and Tokunaga*, 2015], an impact which would certainly influence cyclic flow processes.

Given chemical and geochemical impacts on flow processes, and the complicated hysteretic nature of immiscible flow processes, additional work must be undertaken in order to fully characterize and predict the behavior of cyclic $scCO_2$-brine interactions and $scCO_2$ residual trapping beyond the primary flow processes. This study provides three-dimensional (3-D) pore-scale X-ray computed microtomography (X-ray CMT) visualization of reservoir-condition $scCO_2$ and brine movements, paired with capillary pressure values measured in the bulk fluid phases, in Bentheimer sandstone cores during multiple D-I cycles. Experiments were conducted at the Advanced Photon Source at Argonne National Laboratory; the utilization of synchrotron-based imaging of the experiments allowed for rapid acquisition of high-resolution images of six experiments in Bentheimer sandstone cores. New, unfired Bentheimer cores were utilized for each experiment, and various injection pressure-saturation patterns were investigated.

2. Materials and Methods

2.1. Experimental Procedure

We used the experimental setup and experimental process previously described by Herring *et al.* [*Herring et al.*, 2014]; deviations from that system and the general experimental process for this study are briefly described below. All experiments were conducted under the same temperature and pressure conditions (38°C and 8.3 MPa) which render the CO_2 phase supercritical ($scCO_2$); fluid properties under these conditions are displayed in Table S1 in the supporting information. An updated schematic and detailed description of the experimental process relevant to the experiments reported here are included in the supporting information.

A Bentheimer sandstone core was installed within a hassler-type core holder (Phoenix Instruments; Splendora, TX, United States) with two layers of semipermeable hydrophilic membrane with 1.2 μm pore size (General Electric Company; Fairfield, CT, United States) set flush to the bottom of the core and compressed onto the core axial face by the use of Kalrez® perfluoroelastomer o-rings (McMaster-Carr; Elmhurst, IL, United States). The semipermeable membrane prevents $scCO_2$ breakthrough of the core and allows for drainage to high capillary pressure values even with the relatively short cores (approximately 40 mm long; see Table S2 in the supporting information) used in this study. Additionally, the use of a hydrophilic membrane provides a level of control of the extent of the drainage process; we utilize this capability to manipulate the drainage process during experiments to achieve a range of initial saturations. The core-holder was mounted on the stage in the beamline, and polyether ether ketone (PEEK) material flow lines (IDEX Health & Science

LLC; Oak Harbor, WA, United States) were used to connect the fluid accumulators and pumps to the inlet and outlet ports of the core holder.

Two ISCO pumps (Teledyne ISCO, Lincoln, NE, United States) were used for working fluid control: the pump controlling the CO_2-saturated brine was attached via brine-filled flow lines to the bottom of the core holder; the pump controlling the $scCO_2$ phase was attached via $scCO_2$-filled lines to the top of the core holder. Overburden pressure was applied via a third ISCO pump and was set to 12.4 MPa (1800 PSI) for the duration of the experiment. A differential pressure transducer (Teledyne ISCO, Lincoln, NE, United States) with a range of ±55 kPa (560 cmH$_2$O) was connected to the brine flowline via one port and to the $scCO_2$ flowline on the other, thus providing measurement of the capillary pressure ($P_C = P_{scCO2} - P_{brine}$) of the fluids during experiments. Prior to flow experiments, the core was saturated with CO_2-saturated brine at the experimental conditions of 38°C and 8.3 MPa (Text S1). The $scCO_2$ pump was set to maintain constant pressure at the top port of the core holder for both drainage and imbibition processes. Drainage was conducted by setting the brine pump to constant withdrawal flow rate, and the brine pump was halted once the desired differential pressure value was reached. For imbibition, the brine pump was set to a constant infusion flow rate; approximately 30 pore volumes of CO_2-saturated brine were pumped through the core to establish residual conditions. The D-I cycle was repeated two or three times, depending on beam time constraints. Scans were acquired to characterize the core and/or internal $scCO_2$ phase at several points during experiments: after pressurized saturation but prior to any flow experiments to confirm complete brine saturation of the core (denoted $S_{O,scCO2}$, "original saturation"); after drainage ($S_{Ii,scCO2}$, "initial saturation", where *i* refers to the cycle number); and after imbibition ($S_{Ri,scCO2}$, "residual saturation," where *i* refers to the cycle number). Two scans (at two vertical positions along the core) were acquired for each scanning point and are represented as separate data points in the results presented in section 3.

2.2. X-Ray Microtomographic Image Collection and Data Processing

Tomographic imaging was performed at the GeoSoilEnviroCARS (GSECARS) beamline 13-BMD; details of the beamline configuration have been previously reported [*Rivers et al.*, 1999; *Wildenschild et al.*, 2002, 2005]. All image-based data presented in this study were acquired at a monochromatic energy of 35.9 keV, and were reconstructed into a 3-D volume with GSECARS-developed reconstruction code.

The reconstructed 3-D grayscale volumes were processed using the commercial Avizo™ software suite (details in Text S2 and Figure S3 in the supporting information). A 3-D nonlocal means filter was applied to the raw grayscale data to reduce noise and smooth the images, and simple histogram segmentation was accomplished by setting the threshold equal to a grayscale value corresponding to the local minimum between the $scCO_2$ and solid phases of the grayscale histogram. Postsegmentation noise removal was utilized by removing isolated $scCO_2$-identified clusters smaller than 2.4×10^4 μm^3 (i.e., equivalent to a spherical pore with radius of 18 μm) and also removing cavities (i.e., non-$scCO_2$ identified voxels) from within the $scCO_2$ phase. Quantification of final $scCO_2$ phase volume (fluid-phase saturation), connectivity, and topology was performed on the final denoised, segmented volume.

3. Results and Discussion

Residual $scCO_2$ saturation ($S_{R,scCO2}$) as a function of initial CO_2 saturation ($S_{I,scCO2}$) (i.e., the "trapping curve") is shown for all cycles of all experiments in Figure 1.

We find that residual $scCO_2$ saturations are suppressed during the first drainage-imbibition (D-I) cycle in these experiments, potentially due to the relatively high capillary number of these brine imbibition flows (i.e., logCa = −6.1 and −5.7; see Text S1 and Tables S1 and S2 in the supporting information). However, subsequent cycles were conducted at the same capillary number and yet demonstrate significant increases in residual $scCO_2$ saturations compared to the first D-I cycle and even approach a 1:1 initial-residual saturation relationship. The 1:1 relationship represents 100% trapping efficiency: all of the $scCO_2$ which has been injected and is present at the endpoint of drainage remains stable during imbibition and the full injected volume is completely residually trapped. For repeat cycles, we achieve relatively high $S_{R,scCO2}$ values of approximately 0.50, compared to our first cycle values of 0–0.27 and the first cycle trapping values of 0.35 of *Pentland et al.* [2011], 0.30 of *Saeedi et al.* [2011], and 0.33 of *Krevor et al.* [2012]. Isosurfaces of trapped $scCO_2$ are shown to the right of Figure 1 for one particular experiment (data indicated by circles) for which
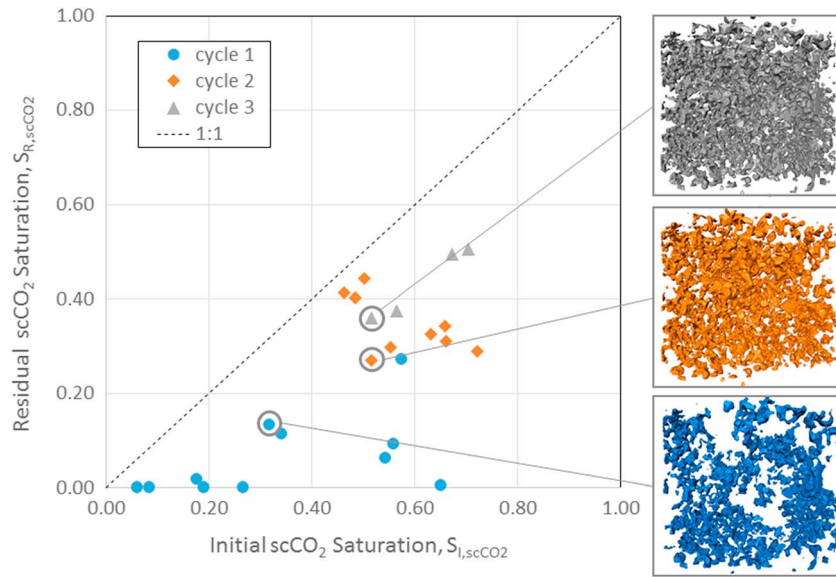
Figure 1. Relationship between residual and initial supercritical CO_2 saturation ($S_{R,scCO2}$ and $S_{I,scCO2}$, respectively). Values are differentiated by cycle number. The dashed line indicates a 1:1 residual-initial relationship, which represents complete trapping (100% trapping efficiency). Three-dimensional visualizations of trapped $scCO_2$ ($S_{R,scCO2}$) for one particular three-cycle experiment are shown to the right; this experiment is further presented in Figure 3.

three D-I cycles were conducted; as shown, trapped $scCO_2$ volume increases with each cycle, even when comparing the results of the second cycle and the third cycle which both show $S_{I,scCO2}$ values of 0.52.

Many previous studies of $scCO_2$-brine floods have reported experimental results suggesting a positive (monotonic) correlation between residual saturation and initial saturation for water-wet media during a single D-I cycle [*Spiteri et al.*, 2005; *Al Mansoori et al.*, 2010; *Pentland et al.*, 2011; *Krevor et al.*, 2012; *Akbarabadi and Piri*, 2013]. For the experiments reported in this study, residual $scCO_2$ saturation increases as cycle number increases for all experiments, but the magnitude of increase is not predicted by a monotonic residual-initial relationship (as demonstrated in Figure 1). Rather, a hysteretic dependency is uncovered: the order and pattern of extent of sequential drainage processes has a significant effect (Figure 2).

In the context of multicyclic flow processes, the initial (postdrainage) state of the multiphase system cannot be identified solely by a single parameter; i.e., saturation and capillary pressure are not single-valued quantities for the drainage process due to the existence of scanning curves. Thus, in order to compare differences between the initial states of the sequential D-I cycles and to acknowledge that our data lie along scanning curves as well as the primary drainage curve, we use the qualitative term "extent of drainage" to express the degree to which $scCO_2$ has invaded the pore spaces of the sandstone medium. We quantify the extent of drainage using four variables: (1) saturation (S_{scCO2}), (2) capillary pressure (P_C), (3) connectivity as measured by the gamma metric (Γ), and (4) topology as measured by the Euler characteristic (χ). A high extent of drainage is associated with high $scCO_2$ saturation, high capillary pressure, and high $scCO_2$ connectivity and topology; but extent of drainage cannot necessarily be determined from any one of these parameters alone. Further, we utilize the term "relative extent of drainage" to describe the difference in drainage extent between the second and first drainage processes (i.e., the difference between the second and first "initial" states).

To demonstrate the hysteretic dependency of the trapping increase, we focus on the results of the second and third D-I cycles in Figure 2. Residual $scCO_2$ saturation ($S_{Ri,scCO2}$) is a function of the difference in drainage extent between the ith and ith − 1 drainage processes. The relative extent of drainage is quantified in Figure 2 via (a) change in initial capillary pressure, ΔP_{CI}; (b) change in initial saturation level, $\Delta S_{I,scCO2}$; (c) change in initial connectivity of $scCO_2$ as quantified by the gamma metric, $\Delta \Gamma_I$; and (d) change in initial topology, or interconnectivity, of $scCO_2$ as quantified by the Euler value, $\Delta \chi_I$. As shown, for higher ΔP_{CI} (i.e., $P_{CIi} > P_{CI(i-1)}$), or for higher $\Delta S_{I,scCO2}$ ($S_{Ii,scCO2} > S_{I(i-1),scCO2}$); the amount of residually trapped $scCO_2$ decreases.
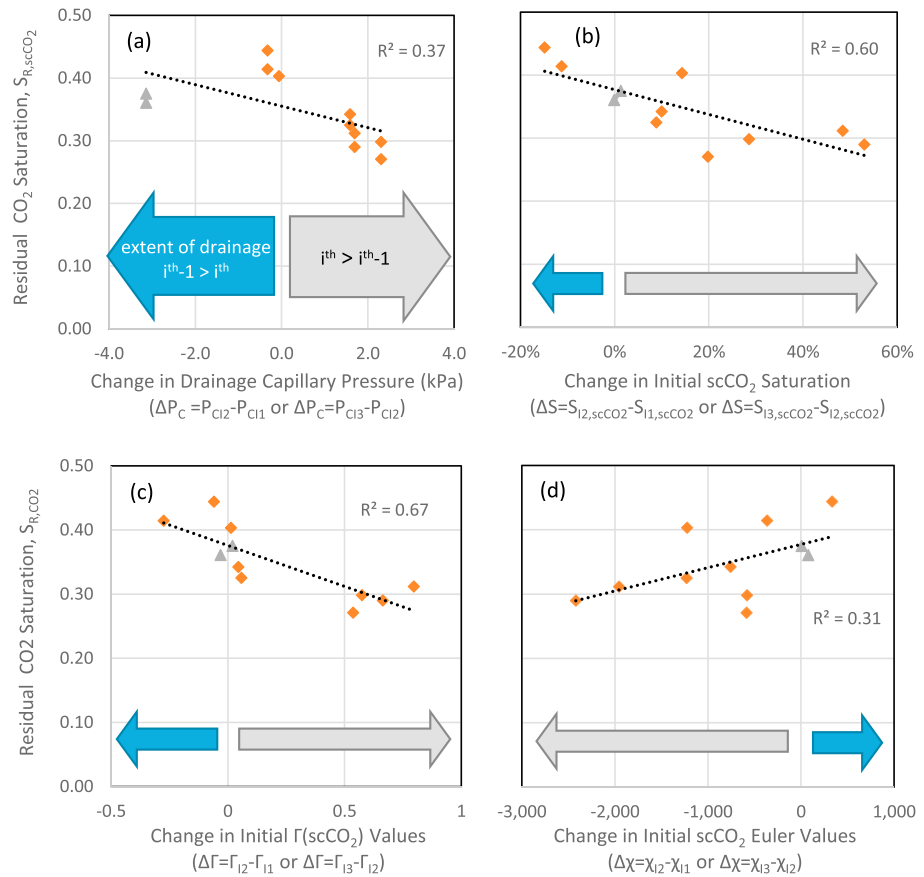
Figure 2. Total residual supercritical CO_2 (scCO_2) saturation of the second drainage-imbibition (D-I) cycle as a function of metrics describing the relative extent of the first (primary; cycle number $i = 1$), second ($i = 2$), and third ($i = 3$) drainage processes. The relative extent of drainage is quantified by the difference between measured quantities at the ith and ith − 1 initial states, i.e., the end of the drainage processes: (a) initial capillary pressure (P_{Cli}); (b) initial scCO_2 saturation ($S_{Ii,scCO2}$); (c) initial connectivity of the scCO_2 phase quantified by Γ_{Ii}; and (d) initial topology of the scCO_2 phase quantified by the Euler number (χ_{Ii}). Gray arrows indicate that the ith drainage process was carried out to greater extent relative to the ith − 1 drainage process, blue arrows indicate that the ith drainage process was carried out to lesser extent relative to the ith − 1 drainage.

That is, if the extent of drainage of the ith cycle is greater than that of the ith − 1 cycle, less total scCO_2 is trapped at the end of the ith D-I cycle. Notably, in Figure 2a, the results for the third cycle do not conform to those for the second cycle; this is potentially due to a shift in capillary pressure relationships over time, an effect which is further discussed in hypothesis (1) below.

This result is corroborated when drainage extent is quantified via scCO_2 connectivity (c) and topology (d): for experiments where the ith drainage process was carried out to greater extent, the initial scCO_2 was better connected relative to the ith − 1 drainage process, and less total scCO_2 is trapped at the end of the ith D-I cycle. The Γ and Euler values have been previously used to quantify fluid connectivity and topology (i.e., interconnectivity), respectively, within porous media [*Vogel et al.*, 2010; *Herring et al.*, 2013, 2014, 2015; *Rücker et al.*, 2015; *Schlüter et al.*, 2016] and are explicitly defined in the supporting information (Text S2). For interpretation of Figure 2 we note that Γ values for fluid within a porous medium range from 0 to 1.0, with 0 representing no connectivity and 1.0 representing maximum connectivity; highly negative Euler values indicate a well-interconnected fluid phase with a high number of internal connections via redundant pore throats, while positive Euler values indicate many disconnected fluid bodies with few redundant internal connections [*Herring et al.*, 2015]. Because Figure 2 presents residual trapping as a function of the *change* in initial state between the ith and ith − 1 D-I cycles, a high $\Delta\Gamma_I$ or highly negative $\Delta\chi_I$ value indicates that the second drainage resulted in a more highly connected initial scCO_2 phase than the first drainage process. As described by *Herring et al.* [2013, 2015], a more highly connected/interconnected nonwetting phase at the postdrainage

stage provides extra redundant "pathways" through which nonwetting phase is likely to be mobilized during imbibition. The trends shown in Figures 2c and 2d thus complement those presented in Figures 2a and 2b, namely, that for experiments where the ith drainage process was carried out to greater extent, the scCO$_2$ demonstrated higher connectivity/interconnectivity, and the total residual scCO$_2$ saturation at the end of the ith cycle is lower.

We hypothesize that a combination of two mechanisms contribute to this hysteretic effect:

1. Time-dependent surface chemistry reactions (e.g., heterogeneous wettability alteration to a more CO$_2$-wet surface, clay mineral dissolution and redistribution, or adhesion of scCO$_2$ to the solid surface as proposed by *Wang and Tokunaga* [2015]) occurred upon prolonged exposure to scCO$_2$, which rendered the scCO$_2$ phase to become increasingly more stable in the pore spaces over time. Pore bodies in which CO$_2$ was trapped during the early cycles were more likely to retain CO$_2$ over subsequent D-I cycles; however, regions which were exposed to CO$_2$ for a shorter time period, or not at all, retained original surface characteristics. As cycle number increased, the solid surface experienced additional contact time with scCO$_2$, and thus, surface reactions progressed further (and occurred on additional surfaces within the sandstone core) each time a D-I cycle was accomplished. Surface chemistry reactions may have also impacted the measured capillary pressure relationships, resulting in a shift in measured values as the experiments progressed (e.g., Figure 2a). In support of this hypothesis, a recent study by *Wang and Tokunaga* [2015] presented similar observations of significant increases in residual trapping (attributed in that study to time-dependent wettability alteration due to scCO$_2$ exposure).

2. Initial state fluid connectivity and topology have been linked to fluid mobilization during imbibition in ambient condition studies [*Herring et al.*, 2013, 2015]. For experiments where the second drainage process was carried out to further extent than the first drainage process (as indicated by the gray arrow in Figure 2), the elevated connectivity of scCO$_2$ at the second initial state enabled the mobilization of previously trapped scCO$_2$, resulting in less residual trapping overall at the end of the second cycle. For experiments where the second drainage process was carried out to lesser extent than the first (as indicated by the blue arrow in Figure 2), the previously trapped scCO$_2$ remained stable, and newly introduced scCO$_2$ only contributed to additional residual trapping.

The combination and potential competition of these two mechanisms explains our observations: temporally, progressive surface chemistry reactions (but only of pore spaces where scCO$_2$ is stable for relatively long timeframes) leads to dramatically increased residual trapping, and high extents of drainage result in more extensive spatial distribution of surface reactions; at the same time, high extent of drainage results in increased connectivity and contributes to mobilization of scCO$_2$. Thus, there are both collaborative and competitive impacts due to surface chemistry and extent of drainage.

Visualization of the cyclic trapping behavior is exhibited in Figure 3 which shows a filtered tomographic cross-sectional slice of a sample over the course of three D-I cycles. In these images, the X-ray attenuating brine appears as light gray, sandstone grains appear as a moderate gray, and scCO$_2$ appears as a darker shade. For this particular experiment, the first drainage was conducted to a moderate capillary pressure (resulting in a low S_{I1,CO_2} value of 0.13); the second was conducted to a high capillary pressure (resulting in a moderate S_{I2,CO_2} value of 0.27, which is the sum of previously trapped scCO$_2$ as well as newly introduced scCO$_2$); and the third drainage to a low capillary pressure (which resulted in a moderate S_{I3,CO_2} value of 0.36, again the sum of previously trapped scCO$_2$ as well as newly introduced scCO$_2$). An orange circle highlights a particular scCO$_2$ ganglion: although trapped after the first D-I cycle (Figure 3b), the second drainage process (Figure 3c) was carried out to a higher extent than the first (Figure 3a), resulting in mobilization of the ganglion during the second imbibition process (Figure 3d). The third drainage process (Figure 3e) was carried out to similar extent relative to the second, but allowed for reentry of the scCO$_2$ to that particular pore body, and subsequent entrapment of the scCO$_2$ ganglion during the third and final imbibition (Figure 3f). Overall, a clear trend of increasing residual saturation as cycle number increases is shown in the cross-sectional slices Figures 3b, 3d and 3f. The capillary pressure-saturation relationship for this particular experiment is included in Figure S4 in the supporting information.

The results and time-dependent surface chemistry hypothesis presented here are supported by dewetting observations in silica micromodels [*Kim et al.*, 2012] and the results of recent flow studies conducted in
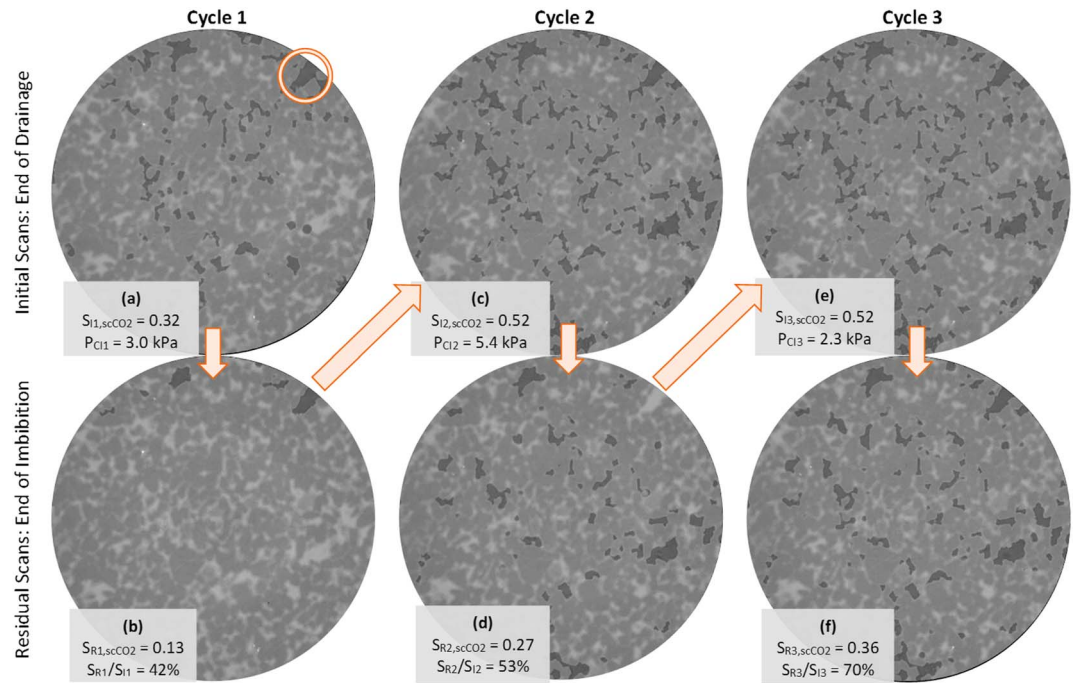
Figure 3. A cross-sectional slice of grayscale data over the course of three drainage-imbibition (D-I) cycles. Highly attenuating 1.0 M KI brine presents as light gray, the sandstone grains appear to be moderate gray, and the lower attenuating supercritical CO_2 (scCO$_2$) phase is identified by the dark gray. (a, c, and e) The core at the end of drainage ("initial state") and (b, d, and f) the same core at the end of the subsequent imbibition ("residual state"); the cycle number (i) increases from left to right. For the initial states, the scCO$_2$ saturation ($S_{Ii,scCO2}$) and drainage endpoint capillary pressure (P_C) are given; For residual states, scCO$_2$ saturation ($S_{Ri,scCO2}$) and trapping efficiency (S_{Ri}/S_{Ii}) are given. The first D-I cycle, Figures 3a and 3b, results in relatively low residual trapping; after the second cycle, Figures 3c and 3d, residual trapping and trapping efficiency increases; and the third cycle, Figures 3e and 3f, results in the highest values for scCO$_2$ trapping and trapping efficiency.

scCO$_2$-aged quartz, limestone, and dolomite sands [*Wang and Tokunaga*, 2015]; but are in contrast to previous multicycle ambient-condition [*Raeesi et al*., 2014] and reservoir-condition [*Saeedi et al*., 2011; *Li et al*., 2015] experiments in sandstones, which have indicated that repeated cycling has no impact on nonwetting phase (air and scCO$_2$) trapping. Differences in observed wettability conditions and trapping behavior could be due to chemical differences in the nonwetting fluids due to different pressure-temperature conditions among the experiments or to different samples or sample preparation methods resulting in different geochemical conditions. As reported by *Wan et al*. [2014], wettability in particular is a notoriously difficult parameter to control in experiments with scCO$_2$ and minor differences in sample preparation could lead to dramatic variations in surface chemistry behavior; in addition, contact order (i.e. whether the first substrate contact was by brine or scCO$_2$), contact time, and number of incidences of scCO$_2$-substrate contacts were also shown to impact contact angle measurements [*Wan et al*., 2014].

While the causes of the discrepancy in trapping behavior between this study and previous research certainly warrant additional investigation, the results provide compelling evidence and motivation for using cyclic injection schemes to enhance trapping and safe storage of CO$_2$ in the subsurface.

4. Conclusions

This study utilized synchrotron X-ray tomographic imaging to demonstrate that use of a cyclic injection scheme significantly increased residual trapping of scCO$_2$ in Bentheimer sandstone cores. The magnitude of increase in scCO$_2$ residual trapping over multiple cycles exhibits a hysteretic dependency: increased total residual scCO$_2$ saturation values are associated with experiments where the first drainage process was carried out to higher extent (drainage performed to relatively high capillary pressure and initial overall saturation of

$scCO_2$) with subsequent drainage processes carried out to lesser extent (drainage performed to relatively low capillary pressure and initial overall saturation of $scCO_2$). However, for all experiments, regardless of pattern of drainage extent, residual $scCO_2$ saturations increased significantly as D-I cycle number increased; indicating that cyclic $scCO_2$ and brine injections may be utilized to increase residual trapping during sequestration operations. Residual $scCO_2$ saturations of up to 0.50 are achieved after the third D-I cycle, significantly higher than any previous reports.

The trapping behavior reported here is not predicted by conventional multiphase theory and suggests that $scCO_2$ exposure may induce time-dependent surface chemistry reactions in certain geologic materials. Additional studies are necessary to fully understand the kinetics of, and underlying mechanisms responsible for, this behavior.

References

Akbarabadi, M., and M. Piri (2013), Relative permeability hysteresis and capillary trapping characteristics of supercritical CO_2/brine systems: An experimental study at reservoir conditions, *Adv. Water Resour.*, *52*, 190–206, doi:10.1016/j.advwatres.2012.06.014.

Al Mansoori, S. K., E. Itsekiri, S. Iglauer, C. H. Pentland, B. Bijeljic, and M. J. Blunt (2010), Measurements of non-wetting phase trapping applied to carbon dioxide storage, *Int. J. Greenhouse Gas Control*, *4*(2), 283–288, doi:10.1016/j.ijggc.2009.09.013.

Al Mansoori, S., S. Iglauer, C. H. Pentland, B. Bijeljic, and M. J. Blunt (2009), Measurements of non-wetting phase trapping applied to carbon dioxide storage, *Energy Procedia*, *1*(1), 3173–3180, doi:10.1016/j.egypro.2009.02.100.

Andrew, M., B. Bijeljic, and M. J. Blunt (2013), Pore-scale imaging of geological carbon dioxide storage under in situ conditions, *Geophys. Res. Lett.*, *40*, 3915–3918, doi:10.1002/grl.50771.

Andrew, M., B. Bijeljic, and M. J. Blunt (2014), Pore-by-pore capillary pressure measurements using X-ray microtomography at reservoir conditions: Curvature, snap-off, and remobilization of residual CO_2, *Water Resour. Res.*, *50*, 8760–8774, doi:10.1002/2014WR015970.

Bachu, S. (2003), Screening and ranking of sedimentary basins for sequestration of CO_2 in geological media in response to climate change, *Environ. Geol.*, *44*(3), 277–289, doi:10.1007/s00254-003-0762-9.

Bachu, S., and B. Bennion (2008), Effects of in-situ conditions on relative permeability characteristics of CO_2-brine systems, *Environ. Geol.*, *54*(8), 1707–1722, doi:10.1007/s00254-007-0946-9.

Benson, S. M., and D. R. Cole (2008), CO_2 sequestration in deep sedimentary formations, *Elements*, *4*(5), 325–331, doi:10.2113/gselements.4.5.325.

Chaudhary, K., M. Bayani Cardenas, W. W. Wolfe, J. A. Maisano, R. A. Ketcham, and P. C. Bennett (2013), Pore-scale trapping of supercritical CO_2 and the role of grain wettability and shape, *Geophys. Res. Lett.*, *40*, 3878–3882, doi:10.1002/grl.50658.

Chaudhary, K., E. J. Guiltinan, M. B. Cardenas, J. A. Maisano, R. A. Ketcham, and P. C. Bennett (2015), Wettability measurement under high P-T conditions using X-ray imaging with application to the brine-supercritical CO_2 system, *Geochem. Geophys. Geosyst.*, *16*, 2858–2864, doi:10.1002/2015GC005936.

El-Maghraby, R. M., and M. J. Blunt (2013), Residual CO_2 trapping in Indiana limestone, *Environ. Sci. Technol.*, *47*(1), 227–233, doi:10.1021/es304166u.

Gunter, W. D., S. Bachu, and S. Benson (2004), The role of hydrogeological and geochemical trapping in sedimentary basins for secure geological storage of carbon dioxide, *Geol. Soc. London, Spec. Publ.*, *233*(1), 129–145, doi:10.1144/gsl.sp.2004.233.01.09.

Herring, A. L., E. J. Harper, L. Andersson, A. Sheppard, B. K. Bay, and D. Wildenschild (2013), Effect of fluid topology on residual nonwetting phase trapping: Implications for geologic CO_2 sequestration, *Adv. Water Resour.*, *62*, 47–58, doi:10.1016/j.advwatres.2013.09.015.

Herring, A. L., L. Andersson, D. Newell, J. W. Carey, and D. Wildenschild (2014), Pore-scale observations of supercritical CO_2 drainage in Bentheimer sandstone by synchrotron X-ray imaging, *Int. J. Greenhouse Gas Control*, *25*, 93–101.

Herring, A. L., L. Andersson, S. Schlüter, A. Sheppard, and D. Wildenschild (2015), Efficiently engineering pore-scale processes: Force balance and topology during nonwetting phase trapping in porous media, *Adv. Water Resour.*, *79*, 91–102, doi:10.1016/j.advwatres.2015.02.005.

Iglauer, S., A. Paluszny, C. H. Pentland, and M. J. Blunt (2011), Residual CO_2 imaged with X-ray micro-tomography, *Geophys. Res. Lett.*, *38*, L21403, doi:10.1029/2011GL049680.

Intergovernmental Panel on Climate Change (2005), *IPCC Special Report on Carbon Dioxide Capture and Storage*, edited by B. Metz et al., Cambridge Univ. Press, Cambridge, U. K.

Juanes, R., E. J. Spiteri, F. M. Orr Jr., and M. J. Blunt (2006), Impact of relative permeability hysteresis on geological CO_2 storage, *Water Resour. Res.*, *42*, W12418, doi:10.1029/2005WR004806.

Juanes, R., C. MacMinn, and M. Szulczewski (2010), The footprint of the CO_2 plume during carbon dioxide storage in saline aquifers: Storage efficiency for capillary trapping at the basin scale, *Transp. Porous Media*, *82*(1), 19–30, doi:10.1007/s11242-009-9420-3.

Kaveh, N. S., E. S. J. Rudolph, P. van Hemert, W. R. Rossen, and K.-H. Wolf (2014), Wettability evaluation of a CO_2/water/bentheimer sandstone system: Contact angle, dissolution, and bubble size, *Energy Fuels*, *28*(6), 4002–4020, doi:10.1021/ef500034j.

Kazemifar, F., G. Blois, D. C. Kyritsis, and K. T. Christensen (2015), Quantifying the flow dynamics of supercritical CO_2–water displacement in a 2D porous micromodel using fluorescent microscopy and microscopic PIV, *Adv. Water Resour.*, doi:10.1016/j.advwatres.2015.05.011.

Kim, Y., J. Wan, T. J. Kneafsey, and T. K. Tokunaga (2012), Dewetting of silica surfaces upon reactions with supercritical CO_2 and brine: Pore-scale studies in micromodels, *Environ. Sci. Technol.*, *46*(7), 4228–4235, doi:10.1021/es204096w.

Krevor, S. C. M., R. Pini, L. Zuo, and S. M. Benson (2012), Relative permeability and trapping of CO_2 and water in sandstone rocks at reservoir conditions, *Water Resour. Res.*, *48*, W02532, doi:10.1029/2011WR010859.

Kumar, A., R. Ozah, M. Noh, G. A. Pope, S. Bryant, K. Sepehrnoori, and L. W. Lake (2005), Reservoir simulation of CO_2 storage in deep saline aquifers, *SPE J.*, *10*(3), 336–348, doi:10.2118/89343-PA.

Li, X., M. Akbarabadi, Z. T. Karpyn, M. Piri, and E. Bazilevskaya (2015), Experimental investigation of carbon dioxide trapping due to capillary retention in saline aquifers, *Geofluids*, *15*(4), 563–576, doi:10.1111/gfl.12127.

Manceau, J. C., J. Ma, R. Li, P. Audigane, P. X. Jiang, R. N. Xu, J. Tremosa, and C. Lerouge (2015), Two-phase flow properties of a sandstone rock for the CO_2/water system: Core-flooding experiments, and focus on impacts of mineralogical changes, *Water Resour. Res.*, *51*, 2885–2900, doi:10.1002/2014WR015725.

Niu, B., A. Al-Menhali, and S. C. Krevor (2015), The impact of reservoir conditions on the residual trapping of carbon dioxide in Berea sandstone, *Water Resour. Res.*, *51*(4), 2009–2029, doi:10.1002/2014WR016441.

Pentland, C. H., R. El-Maghraby, S. Iglauer, and M. J. Blunt (2011), Measurements of the capillary trapping of super-critical carbon dioxide in Berea sandstone, *Geophys. Res. Lett.*, *38*, L06401, doi:10.1029/2011GL046683.

Perrin, J.-C., and S. Benson (2010), An experimental study on the influence of sub-core scale heterogeneities on CO_2 distribution in reservoir rocks, *Transp. Porous Media*, *82*(1), 93–109, doi:10.1007/s11242-009-9426-x.

Pini, R., and S. M. Benson (2013), Simultaneous determination of capillary pressure and relative permeability curves from core-flooding experiments with various fluid pairs, *Water Resour. Res.*, *49*(6), 3516–3530, doi:10.1002/wrcr.20274.

Plampin, M., T. Illangasekare, T. Sakaki, and R. Pawar (2014), Experimental study of gas evolution in heterogeneous shallow subsurface formations during leakage of stored CO_2, *Int. J. Greenhouse Gas Control*, *22*, 47–62, doi:10.1016/j.ijggc.2013.12.020.

Plug, W. J., and J. Bruining (2007), Capillary pressure for the sand-CO_2-water system under various pressure conditions. Application to CO_2 sequestration, *Adv. Water Resour.*, *30*(11), 2339–2353, doi:10.1016/j.advwatres.2007.05.010.

Raeesi, B., N. R. Morrow, and G. Mason (2014), Capillary pressure hysteresis behavior of three sandstones measured with a multistep outflow–inflow apparatus, *Vadose Zone J.*, *13*(3), doi:10.2136/vzj2013.06.0097.

Reynolds, C. A., and S. Krevor (2015), Characterising flow behavior for gas injection: Relative permeability of CO_2-brine and N_2-water in heterogeneous rocks, *Water Resour. Res.*, *51*, 9464–9489, doi:10.1002/2015WR018046.

Reynolds, C., M. Blunt, and S. Krevor (2014), Impact of reservoir conditions on CO_2-brine relative permeability in sandstones, *Energy Procedia*, *63*, 5577–5585, doi:10.1016/j.egypro.2014.11.591.

Rivers, M. L., S. R. Sutton, and P. J. Eng (1999), Geoscience applications of X-ray computed microtomography, in *SPIE's International Symposium on Optical Science, Engineering, and Instrumentation*, pp. 78–86 , International Society for Optics and Photonics, Denver, Colo.

Rücker, M., et al. (2015), From connected pathway flow to ganglion dynamics, *Geophys. Res. Lett.*, *42*, 3888–3894, doi:10.1002/2015GL064007.

Ruprecht, C., R. Pini, R. Falta, S. Benson, and L. Murdoch (2014), Hysteretic trapping and relative permeability of CO_2 in sandstone at reservoir conditions, *Int. J. Greenhouse Gas Control*, *27*, 15–27, doi:10.1016/j.ijggc.2014.05.003.

Saeedi, A., R. Rezaee, B. Evans, and B. Clennell (2011), Multiphase flow behaviour during CO_2 geo-sequestration: Emphasis on the effect of cyclic CO_2–brine flooding, *J. Pet. Sci. Eng.*, *79*(3-4), 65–85, doi:10.1016/j.petrol.2011.07.007.

Schlüter, S., S. Berg, M. Rücker, R. T. Armstrong, H.-J. Vogel, R. Hilfer, and D. Wildenschild (2016), Pore-scale displacement mechanisms as a source of hysteresis for two-phase flow in porous media, *Water Resour. Res.*, *52*, 2194–2205, doi:10.1002/2015WR018254.

Spiteri, E., R. Juanes, M. J. Blunt, and F. M. Orr (2005), Relative-permeability hysteresis: Trapping models and application to geological CO_2 sequestration, in *SPE Annual Technical Conference and Exhibition*, Society of Petroleum Engineers, Dallas, Tex.

Trevisan, L., A. Cihan, F. Fagerlund, E. Agartan, H. Mori, J. T. Birkholzer, Q. Zhou, and T. H. Illangasekare (2014), Investigation of mechanisms of supercritical CO_2 trapping in deep saline reservoirs using surrogate fluids at ambient laboratory conditions, *Int. J. Greenhouse Gas Control*, *29*, 35–49, doi:10.1016/j.ijggc.2014.07.012.

Vogel, H.-J., U. Weller, and S. Schlüter (2010), Quantification of soil structure based on Minkowski functions, *Comput. Geosci.*, *36*(10), 1236–1245, doi:10.1016/j.cageo.2010.03.007.

Wan, J., Y. Kim, and T. K. Tokunaga (2014), Contact angle measurement ambiguity in supercritical CO_2–water–mineral systems: Mica as an example, *Int. J. Greenhouse Gas Control*, *31*, 128–137, doi:10.1016/j.ijggc.2014.09.029.

Wang, S., and T. K. Tokunaga (2015), Capillary pressure-saturation relations for supercritical CO_2 and brine in limestone/dolomite sands: Implications for geologic carbon sequestration in carbonate reservoirs, *Environ. Sci. Technol.*, *49*(12), 7208–7217, doi:10.1021/acs.est.5b00826.

Wang, Y., C. Zhang, N. Wei, M. Oostrom, T. W. Wietsma, X. Li, and A. Bonneville (2012), Experimental study of crossover from capillary to viscous fingering for supercritical CO_2–water displacement in a homogeneous pore network, *Environ. Sci. Technol.*, *47*(1), 212–218.

Wildenschild, D., C. M. P. Vaz, M. L. Rivers, D. Rikard, and B. S. B. Christensen (2002), Using X-ray computed tomography in hydrology: Systems, resolutions, and limitations, *J. Hydrol.*, *267*(3–4), 285–297, doi:10.1016/s0022-1694(02)00157-9.

Wildenschild, D., J. W. Hopmans, M. L. Rivers, and A. J. R. Kent (2005), Quantitative analysis of flow processes in a sand using synchrotron-based X-ray microtomography, *Vadose Zone J.*, *4*(1), 112–126.